Energy & Environmental Science

Accepted Manuscript

ROYAL SOCIETY OF CHEMISTRY

www.rsc.org/ees

Journal Name

ARTICLE

Selective CO Production by Au coupled ZnTe/ZnO in photoelectrochemical CO_2 reduction system

Received 00th January 20xx,
Accepted 00th January 20xx

DOI: 10.1039/x0xx00000x

www.rsc.org/

Youn Jeong Jang[a], Ji-wook Jang[b], Jaehyuk Lee[a], Ju Hun Kim[a], Hiromu Kumagai[c], Jinwoo Lee[a], Tsutomu Minegishi[c], Jun Kubota[c], Kazunari Domen[c], Jae Sung Lee[b]*

Gold-coupled ZnTe/ZnO-nanowire array is a new photocathode for selective CO_2 reduction to CO. At -0.7 V_{RHE} under simulated 1 sun illumination, its photocurrent (-16.0 $mAcm^{-2}$) and incident photon-to- current conversion efficiency (97%) represent the highest among reported ZnTe photocathodes for CO_2 reduction and dramatic enhancement from those of bare electrode (-7.9 $mAcm^{-2}$, 68%). In addition, the Au nanoparticles turn mainly-hydrogen-producing bare ZnTe/ZnO-nanowire into mainly-CO-producing photocathode in photoelectrochemical CO_2 reduction. The remarkable effects of Au co-catalyst originate from the formation of a Schottky junction with ZnTe to improve charge separation and to provide reaction centers of CO_2 reduction suppressing competing water reduction.

BROADER CONTEXT.

Carbon dioxide (CO_2) reutilization is attracting great global attention in recent years to capture the most important greenhouse gas and to convert it into valuable chemicals and fuels. Photoelectrochemical CO_2 reduction using abundant solar light and water is an ideal path to CO_2 reutilization because of cleanness and sustainability of the technology. Unfortunately, however, there are a number of technical barriers to overcome before the practical applications including the low solar energy conversion efficiency of the photoelectrodes and the low selectivity of CO_2-reducing electrocatalyst to a desired product molecule. The Au coupled ZnO/ZnTe composite photocathode reported here demonstrates excellent efficiency and high selectivity of CO_2 reduction to CO. In particular, Au nanoparticles improve photogenerated carrier separation by Schottky junction formation and promote selective CO production suppressing competing water reduction to H_2.

Introduction

Carbon dioxide conversion to clean and renewable chemicals or fuels has received a great deal of attention in recent years as a means of CO_2 reutilization. Although the combustion of these fuels produces CO_2 again, the technologies reduce the rate of new carbon being added to the environment. In addition, they can produce liquid hydrocarbons useful for the transportation industry to decarbonize. Among many possible strategies of CO_2 reduction, the photoelectrochemical (PEC) method is an ideal pathway to reutilize CO_2 as a feedstock for various chemicals and fuels by using abundant solar light and water in a clean and sustainable manner.[1-3]

However, the development of this field has been slow mainly due to inadequate performance of the (photo)electrodes showing a low efficiency, a high overpotential to reduce CO_2, and a low electrical and chemical stability in aqueous electrolyte.[4, 5] Many semiconductor photocathodes have been investigated such as GaP,[1] InP,[6] p-Si,[7] Cu_2O,[8] and $CuFeO_2$,[9] yet there is still no material that is free from those limitations. Another important issue in (photo)electrochemical CO_2 reduction is competition between reduction reactions of CO_2 (to carbon-based chemicals) and water (to hydrogen) due to their similar reduction potentials.[10] The formation of a variety of products by CO_2 reduction is a drawback that could make practical processes complicated with additional costs for separation. The reaction involves multiple proton-coupled electron transfer and overlapped redox potentials to form HCOOH, CO, HCHO, CH_3OH, CH_4 and higher hydrocarbons.[11-13]

ZnTe is a promising p-type semiconductor as a photocathode with many desired properties including the small direct band gap of 2.26 eV to utilize solar spectrum effectively. In particular, its most negative conduction band edge position (−1.63 V_{RHE}) among p-type semiconductors known so far provides a large driving force for electron transfer from semiconductor electrode to acceptors in electrolyte. However, the ZnTe photocathode has not been fully studied as

[a] Department of Chemical Engineering, Pohang University of Science and Technology (POSTECH), San 31 Hyoja-Dong, Pohang, 790-784, Korea
[b] Department of Energy and Chemical Engineering, Ulsan National Institute of Science and Technology (UNIST), 50 UNIST-gil, Ulsan, 689-798 Korea.
[c] Department of Chemical System Engineering, University of Tokyo, 7-3-1 Hongo, Bunkyo-Ku, Tokyo 113-8656, Japan

Electronic Supplementary Information (ESI) available: SEM-EDS results, SEM images, deposited Au size distribution, J-V curves, UV-Vis DRS, Tauc plots, gas evolution test, schematic diagrams for set-up and Schottky junction formation, parameters extracted from EIS, and Chronoampere tests for the samples. See DOI: 10.1039/x0xx00000x

photoelectrodes. The promotion of simultaneous reductions of CO_2 (mainly to CO) and water (to H_2), and thus a low selectivity to CO has been a challenge.[14, 15] Here, we report Au-coupled ZnTe/ZnO-nanowire (NW) heterojunction photocathode for PEC CO_2 reduction for the first time. In an attempt to catalyze selective production of CO, a useful feedstock to produce a number of chemicals and fuels, Au nanoparticles were strategically deposited on to ZnTe/ZnO-NW array because of its high electrocatalytic effect for converting CO_2 to CO [16,17] Thus, Au-coupled composite recorded >10-fold increase in the production of CO with a high faradaic efficiency of ~90% compared with bare ZnTe/ZnO-NW. Also the CO selectivity relative to H_2 was improved by >7.5 fold with Au deposition.

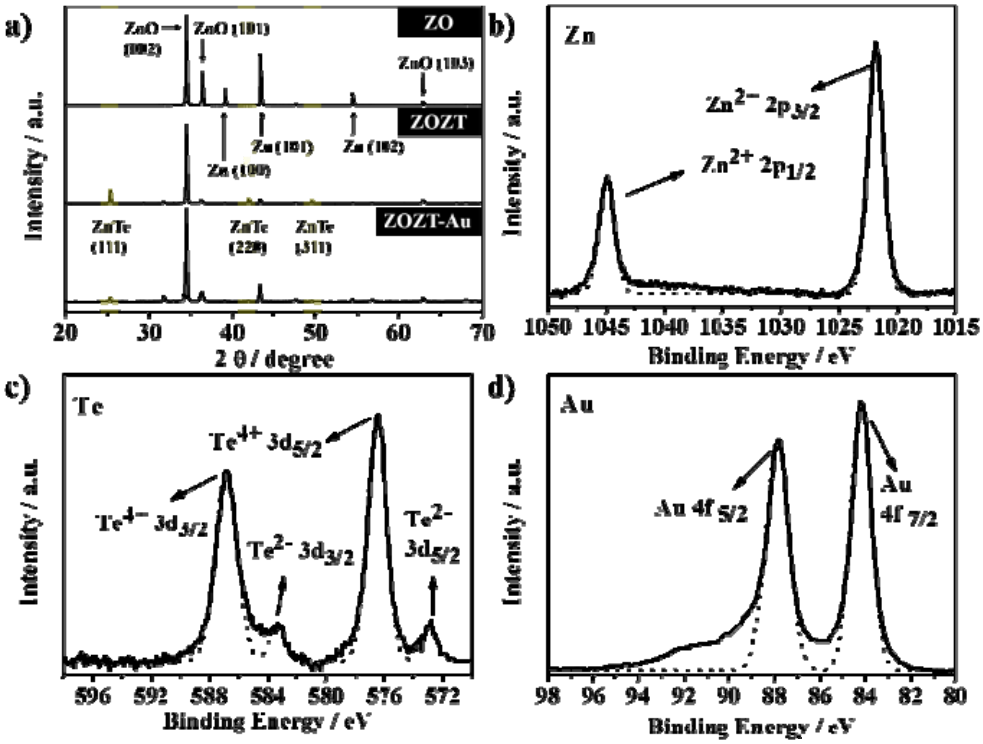

Figure 1. X-ray diffraction patterns of ZnO (denoted as ZO), ZnO/ZnTe (denoated as ZOZT) and Au coupled ZnO/ZnTe (ZOZT-Au) (a), and Core-level X-ray photoelectron spectroscopy (XPS) of Zn 2p (b), Te 3d (c), and Au 4f (d) of ZOZT-Au.

Experimental section

Synthesis of ZnTe/ZnO heterojuntion array.

All chemicals used in this study were of analytical grade and used without further purification. The ZnTe/ZnO photocathode was synthesized by the modified dissolution-recrystallization method. The ZnTe/ZnO electrode was fabricated by two-step. First, ZnO nanowires were synthesized on Zn sheet (Nilaco, 99.5%) in the 10 mM zinc acetate dihydrate ($Zn(CH_3COO)_2{\cdot}2H_2O$, 99%, Aldrich) aqueous solution with ammonia water (NH_3, 28.0–30.0 wt%, Aldrich). The substrate and solution were maintained at 95°C for 1.5 h. After the reaction, the substrate was washed several times with de-ionized water and dried in an oven at 60 °C for 6 h. As a second step, ZnTe crystals were fabricated on the top of ZnO nanowires in an aqueous solution containing 3.6 mM sodium tellurite (Na_2TeO_3, 99%, Aldrich) and 0.66 M hydrazine monohydrate ($N_2H_4{\cdot}H_2O$, Aldrich). The ZnO nanowire array substrate and the solution were loaded into a microwave reactor (Discover SP, CEM Corporation) equipped with a temperature programmer. The solution and the substrate were heated to 195°C within 10 min and maintained at 195°C for 2 h. After reaction, the ZnTe/ZnO substrate was washed several times with de-ionized water, dried at 60°C for 12 h and then annealed at 300°C for 2 h under Ar flow (100 sccm).

Deposition of Au nanoparticle on ZnTe/ZnO heterojunction array.

Au-nanoparticles (NPs) were deposited onto the ZnTe/ZnO substrate by e-beam evaporator (Temescal, USA) at substrate temperature of 250°C and deposition rate of 0.02 nm/s in 1.6×10^{-4} Pa vacuum chamber. The size distribution of Au nanoparticles was controlled by the deposition time after opening the shutter of the system and by a calibrated quartz crystal reference. This procedure enable the control of the nanoparticle size around 2-5 nm. Then the Au deposited ZnTe/ZnO was annealed at 300°C for 1 h under N_2 flow (100sccm)

Photoelectrochemical reduction of CO_2.

The photoelectrochemical performance of the electrodes was measured in a three-electrode system under front-side illumination from a solar simulator (91-160, Oriel) with an air

mass 1.5G filter. The simulated light intensity was calibrated to 1 sun (100 mWcm^{-2}) using a reference guaranteed by National Renewable Energy Laboratories, U.S. The Ag/AgCl electrode in saturated KCl was used as a reference electrode and Pt mesh was used as a counter electrode. The electrolyte was CO_2-saturated 0.5 M potassium bicarbonate (Wako, 99.9%) solution with a pH of 7.5. The photo-activated CO_2 reduction was measured under chopped illumination for observing the photo-response under dark and light simultaneously.

A potentiostat (Gamry Reference 600TM) applied an external bias potential to the system and the scan rate for the linear sweep voltammetry was 5 mVs^{-1}. The gas evolution by photoelectrochemical CO_2 reduction was measured in the same system (Scheme 1 in Electronic Supporting Information, ESI). An Agilent Model 7890 gas chromatography with a Carboxen 1000 packed column and thermal conductivity detector (TCD) was used for the analysis. The gaseous samples were tested for potential products of CO_2 reduction such as CO, methane, ethylene and ethane by injecting onto the gas chromatography. Agilent poraplot-Q capillary column was employed for testing the liquid products for methanol and ethanol with an FID detector. An attempt to measure the quantity of HCOOH was made by high resolution liquid chromatography (HPLC; Agilent 1200) using C18-inverse column.

The incident photon-to-current conversion efficiency (IPCE) was measured using a Xe lamp (300 W, Oriel) and a monochromator with a bandwidth of 5 nm. The IPCE was measured at −0.7 V *vs.* RHE in a 0.5M CO_2-saturated potassium bicarbonate solution (pH 7.5). Potentiostatic electrochemical impedance spectroscopy (EIS) was carried out at -0.7 V *vs.* RHE of DC potential and AC potential frequency range from 100,000 to 0.1 Hz with 10 mV amplitude. The Z-View software (Scribner Associates Inc.) was used to fit obtained data to the corresponding equivalent circuit model.

Characterization of physical properties.

The morphology, crystallinity, and optical properties of the samples were characterized by field-emission scanning electron microscopy (FESEM, JEOL JMS-7401F and Philips Electron Optics B. V. XL30S FEG, operated at 10 keV), X-ray diffraction spectrometry (XRD, Mac Science, M18XHF using Cu Kα radiation, λ = 0.15406 nm), high-resolution transmission electron microscopy (HR-TEM, Cs-corrected, JEOL JEM-2200FS and UV-Vis diffuse reflectance spectroscopy (UV-vis DRS, Shimadzu, UV2501PC).

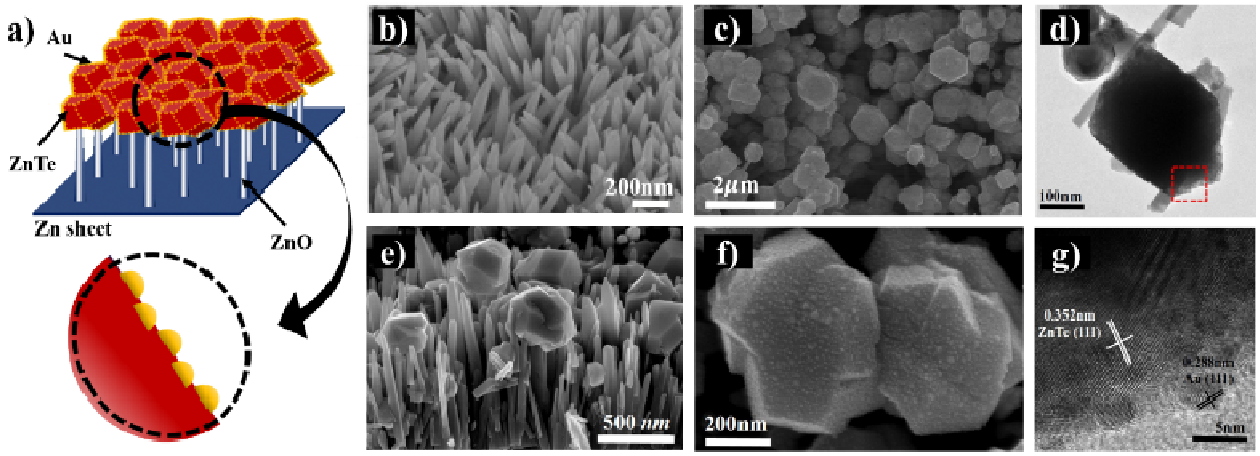

Figure 2. (a) A schematic illustration of Au coupled ZOZT composite. The top view of scanning electron microscopy (SEM) images for ZnO-NW (b) and ZnTe/ZnO-NW (c). (d) The high resolution transmission microscopy (HR-TEM) of Au coupled ZnTe/ZnO-NW. (e) Cross- section SEM image of ZOZT during the dissolution-recrystallization step at 195 °C. (f) The enlarged SEM image of ZOZT-Au. (g) HR-TEM image of the area indicated by the red square in (d).

Results and Discussion

Fabrication of Au-coupled ZnTe/ZnO nanowire array of tulip-like morphology

The fabrication of Au-coupled ZnTe/ZnO-NW composite photocathode starts from growth of ZnO nanowires on a Zn sheet. ZnTe is directly formed on the ZnO nanowires by a modified microwave hydrothermal reaction.[14] The ZnO nanowires act as a Zn source for ZnTe, as well as a bridge for photogenerated charge transfer to provide a remarkably high performance compared to previous reports.[15, 18] The X-ray diffraction (XRD) pattern of the ZnO nanowires on Zn substrate (denoted as ZO) shows both Zn (JCPDS no. 03-065-3358) and hexagonal wurtzite structures of ZnO peaks (JCPDS no. 01-089-0511) in Figure 1a. The XRD peaks of ZnTe/ZnO-NW composite (ZOZT) indicate formation of the zinc-blende ZnTe (JCPDS no. 01-065-0385) on the Zn/ZnO-NW substrate. Au-deposited ZnTe/ZnO-NW (ZOZT-Au) shows similar XRD pattern to ZOZT due to small amount and sizes of gold nanoparticles deposited on the substrate. The gold deposition was confirmed by the point energy dispersive spectroscopy analysis on the scanning electron microscopy (SEM-EDS), which provides more localized element information on Zn, O, Te and Au as shown in Figure S1 in ESI. The X-ray photoelectron spectroscopy (XPS) analysis indicated metallic Au (Au^0), Zn^{2+} from ZnO-NW and ZnTe, and O^{2-} from ZnO-NW as in Figure 1b-d. Both Te^{2-} from ZnTe and Te^{4+} from TeO_2 were observed due to superficial oxidation by exposure to air.[19]

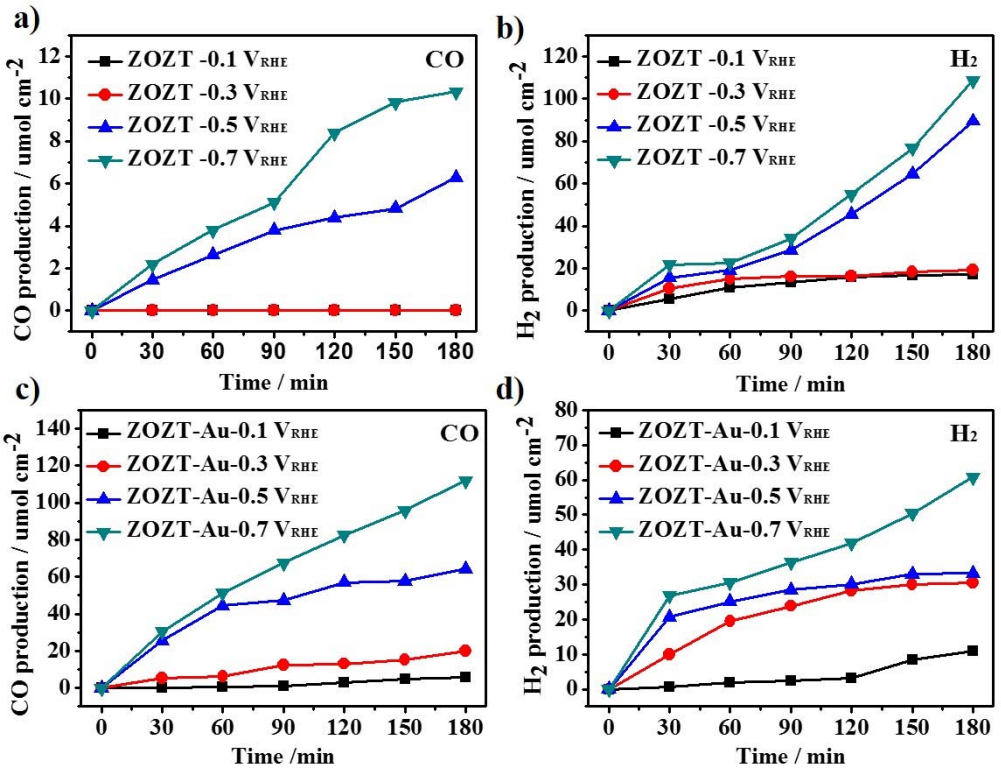

Figure 3. (a) UV-vis absorption of ZnO-NW (ZO), ZnTe/ZnO-NW (ZOZT) and Au decorated ZnTe/ZnO-NW (ZOZT-Au). The inset shows photographs of ZO, ZOZT, and ZOZT-Au. (b) Photocurrent (J) - applied potential (V) characteristics of photocathodes with Pt anode and Ag/AgCl reference electrode in 0.5M $KHCO_3$ under 1 sun illumination at a scan rate of 5 mV/s. (c) IPCE measured at -0.7 V_{RHE}. (d) Nyquist plots of potentiostatic electrochemical impedance spectroscopy (EIS) of bare and Au coupled ZOZT.

Figures 2b shows the scanning electron microscopy (SEM) image of needle shape ZnO nanowires aligned vertically on the Zn sheet (ZO). The ZnO nanowires are capped with broken and Figure S2 (ZOZT). The Figure S3 of ESI shows the SEM images of overlapped cubic shape ZnTe crystallites in Figure 2c and the early stage of ZnTe formation process where ZnTe blocks cover only the top of ZnO nanowires.

Also, the cross-section image of ZnTe/ZnO-NW at the edge of substrate (Figure 2e) reveals the tulip-like morphology schematically illustrated in Figure 2a. The surface of ZnTe is covered with Au nanoparticles of 2-5 nm size after Au e-beam evaporation in Figure 1f (ZOZT-Au). The size distribution of deposited Au nanoparticles is presented in Figure S4 of ESI. Figure 2g shows a high-resolution transmission electron microscopy (HR-TEM) image of the ZnTe grain and Au particles on the area marked in Figure 2d. A lattice spacing of 0.352 nm corresponds to the distance of the (111) lattice planes of zinc-blende ZnTe crystals.[20] In addition, Au nanoparticles show the (111) lattice plane with lattice spacing of 0.288nm.[21, 22] As mentioned, Au nanoparticles sit on the surface of single crystalline ZnTe/ZnO-NW composite.

The mechanism of ZnTe/ZnO-NW composite formation involves dissolution-recrystallization.[14, 23, 24] In hydrazine-containing alkaline solution, $Zn(OH)_4^{2-}$ ion is formed locally on the surface of ZnO-NW by reaction with hydroxyl anions (reaction 1).

$$ZnO_{surface} + H_2O + 2OH^- \rightarrow Zn(OH)_4^{2-} \quad (1)$$

Simultaneously, highly active Te^{2-} ions are released by hydrazine-assisted reduction of tellurite (TeO_3^{2-}) ions through formation of reduced form, Te, as temperature increased (reaction 2, 3).

$$TeO_3^{2-} + N_2H_4 \rightarrow Te + N_2 + H_2O + 2OH^- \quad (2)$$

$$3Te + 6OH^- \rightarrow 2Te^{2-} + TeO_3^{2-} + 3H_2O \quad (3)$$

Then the Te^{2-} ions react with $Zn(OH)_4^{2-}$ to form ZnTe crystals on ZnO-NW by heterogeneous nucleation and growth.[25]

$$Te^{2-} + Zn(OH)_4^{2-} \rightarrow ZnTe + 4\ OH^- \quad (4)$$

The time course of the ZnTe crystals formation was followed by SEM analyses as shown in Figure S3 of ESI. As the reaction proceeds, the size and number of ZnTe crystals increase that grow on the top of ZnO-NW. The observation indicates the larger ZnTe crystals grow upon sacrificing the smaller ZnTe via the typical Ostwald ripening with secondary nucleation and growth.[23]

The UV-Vis diffuse reflectance spectra (UV-vis DRS) in Figure 3a reveal significant differences in the absorption properties. ZO shows a strong absorption in the UV light region characteristic of the wide band gap ZnO with white colour. However, ZOZT and ZOZT-Au show dramatically shifted absorption into the visible light region (<550 nm). The optical band gap energies of ZO, ZOZT, and ZOZT-Au composites were estimated from the Tauc plots in Figure S5: $\alpha\ h\upsilon = A\ (h\upsilon - E_g)^{n/2}$ where α, $h\upsilon$, A, and E_g are an absorption coefficient, the photon energy, a proportional constant and the optical band gap energy, respectively. The obtained optical band gap energy of ZOZT was ~2.25 eV in agreement with the values

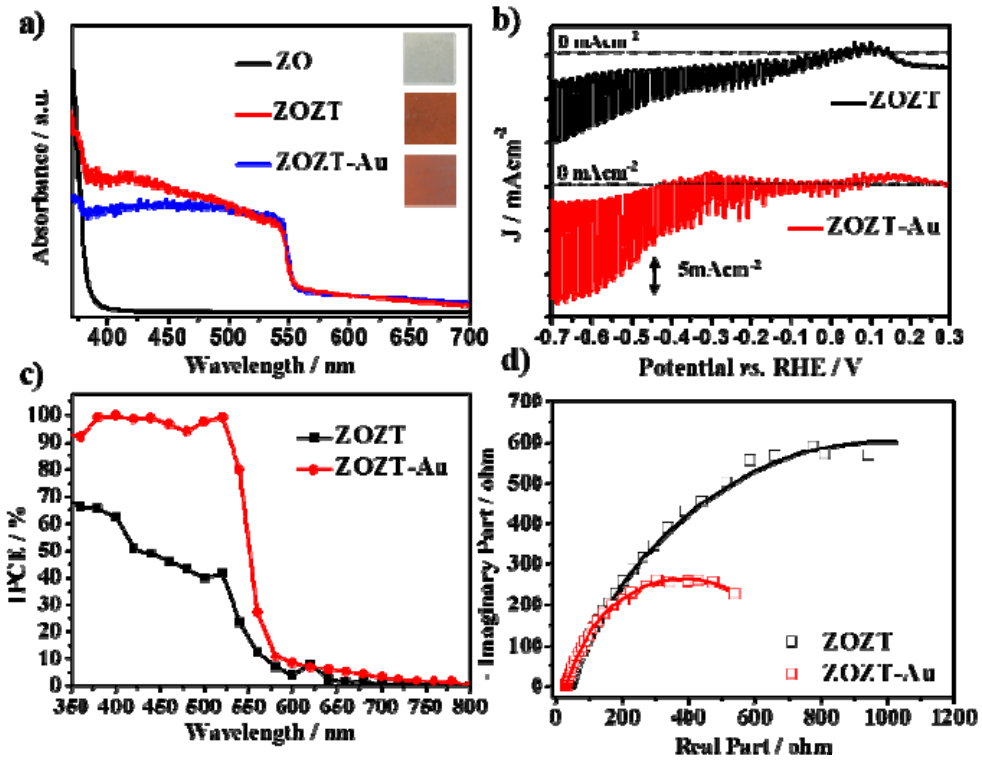

Figure 4. Time-profiled production of CO and H_2 for the ZOZT (a and b, respectively) and for the ZOZT-Au (c and d, respectively) in CO_2-pursed 0.5M $KHCO_3$ electrolytes under simulated 1sun illumination at various applied potentials: -0.1, -0.3,-0.5 and -0.7 V_{RHE}.

reported for ZnTe in literature (2.1~2.26 eV).[26] The optical properties of ZOZT and ZOZT-Au are very similar, *i.e.* reddish reflecting colour, light absorption spectra and Tauc plots. The light absorption of ZOZT-Au is lower than that of ZOZT due to reduced light penetration by in presence of Au particles. The ZnTe/ZnO-NW-Au with larger Au particle sizes around 5-10nm formed by heavier Au loadings shows further reduced light absorption in Figure S6.

Photoelectrochemical reduction of CO_2

Both bare and Au-decorated ZnTe/ZnO-NW were employed as a photocathode for photoelectrochemical CO_2 reduction with a Pt mesh as an anode under irradiation of simulated AM 1.5 G (1 sun) solar light in a typical three-electrode photoelectrochemical system schematically shown in Scheme S1. All the measurements were evaluated under chopped irradiation, so the dark and light current-voltage could be monitored simultaneously. The photocathodes were scanned only below 0.3 V_{RHE} because no cathodic photocurrents were generated above it. The size of Au nanoparticles was controlled by the deposition time and an optimized sample had 2-5 nm Au nanoparticles as in Figure S7. As shown in Figure 3b, photocurrent of the Au coupled ZnTe/ZnO-NW (-3.14 $mAcm^{-2}$) was *ca*. 1.5 times as high as that of bare ZnTe/ZnO-NW electrode (-2.12 $mAcm^{-2}$) at -0.11 V_{RHE} (the theoretical potential necessary for CO production from CO_2). The photoactivity of ZOZT-Au at -0.11 V_{RHE} is compared favourably with other photocathodes reported in the literature including Au/pSi (-1.87 $mAcm^{-2}$), Cu/pSi (ca. 1 $mAcm^{-2}$), and Sn/pSi (ca. -0.5 $mAcm^{-2}$).[4,7,27] At -0.5 V_{RHE} (390 mV overpotential), the ZOZT-Au recorded a drastically enhanced photocurrent of -13.4 $mAcm^{-2}$. On the other hand, the photocurrent of bare ZOZT was -5.6 $mAcm^{-2}$ at the same applied potential. For comparison, the ZnO and Au coupled ZnO electrodes were applied to photoelectrochemical CO_2 reduction, which showed negligible performance due to n-type semiconductor property of ZnO (Figure S8).[14] The result demonstrates that the observed photocatalytic performances of ZnTe/ZnO are originated mainly from ZnTe. In addition, ZnTe and Au coupled ZnTe photocathodes fabricated without ZnO by chemical bath deposition method were also tested for photoelectrochemical CO_2 reduction as shown in Figure S9 and S10. They showed a significant CO_2 reduction activity but their activity and faradaic efficiency were much lower than those of ZnTe/ZnO or Au coupled ZnTe/ZnO. The results indicate that the role of ZnO is not limited to a sacrificial material to form ZnTe, but serves as a charge transport medium to reduce the generated charge recombination and enhance photocatalytic performances.

Incident photon-to-current conversion efficiency (IPCE) in Figure 3c represents the photocathodic response as a function of incident light wavelength: IPCE = [J×1240] / [P_{mono} λ] where J = photocurrent density ($mAcm^{-2}$), P_{mono} = light power density ($mWcm^{-2}$) at λ, and λ = wavelength of incident light (nm). The photocathodes were held at -0.7 V_{RHE} under irradiation with a 300W Xe lamp coupled with a monochromator. Both photocathodes show the onset of IPCE around 550nm as expected from the band gap of ZnTe, ~2.25 eV. The IPCE of

photocathodes followed the UV-vis DRS pretty well, implying that the generated photocurrents by CO_2 reduction were derived from the absorbed light at different wavelengths. The Au coupled ZnTe/ZnO-NW composite marked higher IPCE values compared the bare electrode over all wavelengths, indicating that the photogenerated charge transfer and its separation in ZOZT-Au was better than that in ZOZT as discussed below. The maximum IPCE value of ZOZT-Au photocathode was >97%, whereas the bare ZOZT photocathode recorded 68% in the range of 350–550 nm. The relative values of IPCE for both photocathodes are consistent with the photocurrent results in Figure 3b.

To elucidate the origin of the different photoelectrochemical responses of the ZOZT-Au and ZOZT, we performed potentiostatic electrochemical impedance spectroscopy (EIS) measurements at -0.7 V_{RHE} under the 1-sun condition. The Nyquist plots of both photocathodes are presented in Figure 3d. The data were fitted to a simple equivalent circuit model of two RC circuits made of resistance (R) and constant phase element (CPE) in Figure S11. The RC circuit represents an interface between electrode and electrolyte (R2/CPE2) and the electron pathway within the bulk of the electrode (R1/CPE1). The Rs represents sheet resistance in a half cell test system.[28,29] In general, the largest resistance in RC circuit is observed at electrode/electrolyte interface (R2/CPE2) due to the large charge transfer resistance and double layer capacitance. For the ZOZT-Au photocathode, R2 was reduced by ~2.7 times and CPE2 increases by 2.8 times relative to the bare ZOZT photocathode, indicating that CO_2 reduction occurred more efficiently mainly by improved charge transfer across the electrode/electrolyte interface. In contrast, R1/CPE1 circuit did not show any significant difference indicating that Au modification did not influence the bulk properties of the electrodes.

Let us consider then how Au brings such a remarkable improvement in photoresponse of CO_2 reduction. A possibility to consider is the surface plasmon resonance (SPR) by Au particles, which gives rise to a sharp and intense absorption band in the visible range because of a collective resonant oscillation of the free electrons of the conduction band of the metal.[30] However, UV-Vis absorption and IPCE spectra in Figure 3a,c does not show any sign of SPR. The absence of the SPR effect is believed to be due to the small sizes of our Au particles (2-5 nm) because the strong SPR by Au naoparticles is usually observed for larger Au particles of 5~20 nm.[30-33] Instead, the primary role of Au seems to modify band profile of ZnTe by forming a metal-semiconductor junction. The ZnTe with gold forms a Schottky junction because of smaller work function of Au (5.1-5.3) than that of p-type ZnTe (5.79).[34-37] The Schottky junction causes enhanced band bending of ZnTe into electrolyte, thus photo-generated holes easily migrate into the inside of the electrode and electrons come out to the surface and are transferred through Au into electron acceptor (CO_2 or H^+) in the electrolyte for the reaction as illustrated in Figure S12. This enhanced charge separation leads to the high photoelectrochemical activity. The effect of band bending modulation is limited to a region of the direct metal-semiconductor contact. But if the area of the contact is too large by heavy loading, it would block a part of light absorption. Thus, an optimal Au loading that gave the best photoelectrochemical performance was determined to be *ca*. 0.5 wt%, which formed 2-5 nm Au particles as shown in Figure S7. The loaded amount of Au on ZnTe/ZnO-NW was determined by inductively coupled plasma atomic emission spectroscopy (ICP-AES).

Another critical role of Au was on the selectivity of the CO_2 reduction products. A variety of the products are expected from CO_2 reduction such as H_2, CO, HCOOH, CH_3OH, and so on, due to their similar redox potentials. Deposition of Au nanoparticles improved the selectivity of CO production with negligible other carbon-containing products. Thus photoelectrochemical CO_2 reduction was carried out in $KHCO_3$ electrolyte at −0.7, −0.5, −0.3 and −0.1 V_{RHE} for 3 h as presented in Figure 4. The amounts of generated CO and H_2, their faradaic efficiencies, and selectivity of CO are summarized in Figure 5 and Table 1. The amounts of formed CO increased with the increase of biased potential. In particular, Au loading on ZOZT increased the production of CO by a factor of >10 and reduced the faradaic efficiency for H_2 to less than a half.

Thus, the faradaic efficiency of CO production was enhanced to 26.0 – 63.0 % compared with that of bare ZOZT (0 – 7.2 %) as in Table 1. Bare ZOZT is mainly a water reduction (to H_2) photocatalyst, which turns to CO_2 reduction (to CO) photocatalyst by incorporating Au as a co-catalyst. Au metal favours initial reduction from adsorbed CO_2 into the $CO_2^{\cdot-}{}_{(ads)}$, which is an activated form of CO_2 reduction with carbon atom bonded to surface Au atom.[11-13, 16, 38] Then the proton in the electrolyte reacts with oxygen atom in the activated $CO_2^{\cdot-}{}_{(ads)}$ to form $HOCO_{(ads)}$, which is then reduced to OH and $CO_{(ads)}$ by transferred photogenerated electron.[38] The CO is easily desorbed from the surface of Au.[16] The facile adsorption of $CO_2^{\cdot-}$ effectively suppresses the H^+ adsorption and direct reduction to H_2.

As shown by chronoamperemetry in Figure S13, the photocurrent generation by CO_2 reduction was quite stable at least for 180 min of the test. Also, the morphology of ZnTe crystals was almost preserved during the chronomamperemetry test at -0.7 V_{RHE} although some Au nanoparticles were aggregated and detached from ZnTe like shown in Figure S14. ZOZT-Au showed higher combined faradaic efficiencies than those of bare ZOZT in Table 1. The combined faradaic efficiencies of ZOZT-Au were higher than 90% at high potentials, but were still lower than 100%. Since no other products were detected by GC-FID and HPLC analyses of reaction solution and there were small dark currents observed in Figure 3b, we concluded that aggregation, detachment of Au nanoparticles from ZOZT and non-negligible electrochemical corrosion of ZnO and ZnTe took place due to, for instance, ZnO and ZnTe decomposition into Zn, H_2O and Te^{2-}.[14,39,40] The stability could be further improved by combining with a protective surface layer or a more active electrocatalyst.[27]

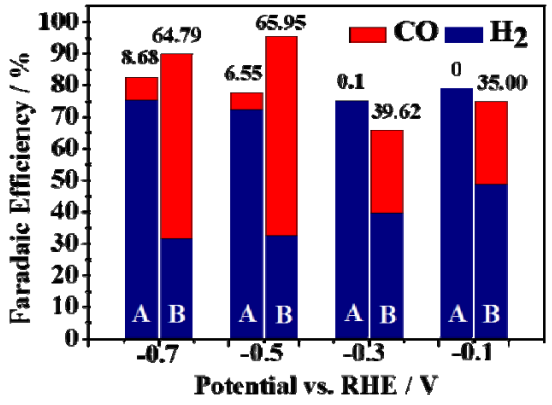

Figure 5. Faradaic efficiencies of CO and H_2 for bare ZOZT (A) and Au decorated ZOZT (B) at different applied potentials in the CO_2-saturated $KHCO_3$ electrolyte under simulated 1sun illumination for 3 h operation. The values above the top of each column present the selectivity of CO from CO_2 reduction relative to H_2 from H_2O. See Table 1 for details.

Table 1. Photoelectrochemical CO_2 reduction[a]

	Potential vs. RHE / V	Amounts of gas product / μmol cm^{-2}		Faradaic efficiency / %			Selectivity of CO / %
		H_2	CO	H_2	CO	Overall	
ZOZT	-0.1	17.0	0.0	79.0	0.0	79.0	0.0
	-0.3	19.2	0.0	75.0	0.1	75.1	0.1
	-0.5	89.5	6.3	72.3	5.1	77.4	6.6
	-0.7	108.7	10.3	75.3	7.2	82.4	8.7
ZOZT -Au	-0.1	10.8	5.8	48.7	26.2	75.0	35.0
	-0.3	30.6	20.1	39.7	26.0	65.7	39.6
	-0.5	33.1	64.2	32.5	63.0	95.5	66.0
	-0.7	60.9	112.0	31.8	58.0	89.9	64.9

[a] In electrolyte of a CO_2 saturated 0.5 M $KHCO_3$ under AM 1.5G light (100 mWcm^{-2}) at the various applied potentials for 3 hr. The faradaic efficiencies of CO and H_2 production are obtained assuming that CO and H_2 production needs two-electron transfer.

Conclusions

Au nanoparticle-coupled ZnTe/ZnO array is an attractive photocathode to convert CO_2 selectively to CO. Its photocurrent (-15.97 mAcm^{-2}) and IPCE value (97%) at -0.7 V_{RHE} under simulated 1 sun illumination represent the highest among reported ZnTe photocathodes for CO_2 reduction and dramatic enhancement from those of bare ZnTe/ZnO electrode (-7.89 mAcm^{-2}, 68%). Interestingly, the Au nanoparticles turn mainly-hydrogen-producing ZnTe/ZnO into mainly-CO- producing photocathode in photoelectrochemical CO_2 reduction by greatly enhancing CO selectivity. The obtained Au coupled ZnTe/ZnO-NW exhibited at least two attributes highly desirable for efficient photoelectrodes with selective CO production: i) The formation of a Schottky junction at the interface between Au particle and ZnTe that allows improved band bending, facile charge separation and electron transfer into electrolyte. ii) The deposited Au nanoparticles provide reaction centres of CO_2 reduction suppressing competing water reduction. There is scope for improvement in electrochemical stability by combining with a protective surface layer or a more active electrocatalyst.

Acknowledgements

This work was supported by Brain Korea Plus Program of Ministry of Education, Korean Centre for Artificial Photosynthesis (NRF-2011-C1AAA0001-2011-0030278) funded by MISIP and Project No. 10050509 funded by MOTIE of Republic of Korea. It was also supported by Ulsan National Institute of Science and Technology (UNIST).

Y.J. Jang carried out photoelectrochemical CO_2 reduction experiments. Y.J. Jang and Dr. J.-W. Jang fabricated the ZnO/ZnTe electrode. Dr. J. Lee carried out characterization such as SEM, TEM, and XRD experiments. J.H. Kim collected x-ray photoelectron spectroscopy data. H. Kumagai, Prof. T. Minegishi, Prof. J. Kubota and Prof. K. Domen helped synthesis of Au nanoparticle, its deposition and characterization. Prof. J. Lee helped set up CO_2 reduction test. All authors participated in data analysis. Prof. J.S. Lee supervised the project. Prof. J.S. Lee and Y.J. Jang co-wrote the manuscript. All authors viewed and commented on the manuscripts.

Notes and references

1 M Halmann, *Nature,* 1978, **275**,115.
2 T. Inoue, A. Fujishima, S. Konishi, K. Honda, *Nature,* 1979, **277**, 637.
3 M. Azuma, K. Hashimoto, M. Hiramoto, M. Watanabe, T. Sakata, *J. Electrochem. Soc.* 1990, **137**, 1772.
4 R. J. Lim, M. Xie, M. A. Sk, J. –M. Lee, A. Fisher, X. Wang, K. H. Lim, *Catal. Today,* 2014, **233**, 169.
5 B. Kumar, M. Llorente, J. Froehlich, T. Dang, A. Sathrum, C. P. Kubiak, *Annu. Rev. Phys. Chem.* 2012, **63**, 541.
6 B. A. Parkinson, P.F. Weaver, *Nature* 1984**, 309**, 148.
7 R. Hinogami, Y. Nakamura, S. Yae, Y. Nakato, *J. phys. Chem. B* 1998, **102**, 974.
8 G. Ghadimkhani, N.R. de Tacconi, W. Chanmanee, C. Janaky, K. Rajeshwar, *Chem. Commun.* 2013, **49**, 1297.
9 J. Gu, A. Wuttig, J. W. Krizan, Y. Hu, Z. M. Detweiler, R. J. Cava, A. B. Bocarsly, *J. Phys. Chem. C,* 2013, **117**, 12415.
10 E. E. Benson, C.P. Kubiak, A. J. Sathrum, J. M. Smieja, *Chem. Soc. Rev.* 2009, 89.
11 D. P. Summers, S. Leach, K. W. Frese Jr, *J. Electroanal. Chem. Interfacial Electrochem.* 1986, **205**, 219.
12 M. Gattrell, N. Gupta, A. Co, *J. Electroanal. Chem.* 2006, **594**, 1.
13 Y. B. Vassiliev, V. S. Bagotzky, N. V. Osetrova, A. A. Mikhailova, *J. Electroanal. Chem. Interfacial Electrochem.* 1985, **189**, 311.
14 J.-W. Jang, S. Cho, G. Magesh, Y. J. Jang, J. *Chem. Int. Ed.* 2014, **126**, 5962.
15 D. H. Won, J. Chung, S. H. Park, E. –H. Kim, S. I. Woo, *J. Mater. Chem. A,* 2015, **3**, 1089.
16 Y. Hori, H. Wakebe, T. Tsukamoto, O. Koga, *Electrochim. Acta* 1994, **39**, 1833.
17 M. D. Dry, *Catal. Today*, 2002, **71**, 227.
18 Y. Lin, W. –J. Chen, J. Lu, Y. Chang, C. –T. Liang, Y. Chen, J. –Y. Lu, *Nanoscale Res. Lett.* 2012, **7**, 1.
19 R. Nayak, V. Gupta, A. L. Dawar, K. Sreenivas, *Thin Solid Films* 2003, **445**, 118.
20 S. H. Lee, Y. J. Kim, J. Park, *Chem. Mater.* 2007, **19**, 4670.

21 M. Torrell, R. Kabir, L. Cunha, M. I. Vasilevskiy, F. Vaz, A. Cavaleiro, E. Alves, N. P. Barradas, *J. Appl. Phys.* 2011, **109**, 074310.
22 D. Gaspar, A. C. Pimentel, T. Mateus, J. P. Leitao, J. Soares, B. P. Falcao, A. Araujo, A. Vicente, S. A. Filonovich, H. Aguas, R. Martins, I. Ferreira, *Sci. Rep.* 2013**, 3**, 1469.
23 S. Cho, J. –W. Jang, J. Kim, J. S. Lee, W. Choi, K. –H. Lee, *Langmuir* 2011, **27**, 10243.
24 S. Cho, J. –W. Jang, S. –H. Lim, H. J. Kang, S. –W. Rhee, J. S. Lee, K. –H. Lee, *J. Mater. Chem.* 2011, **21**, 17816.
25 S. Xu, C. Wang, Q. Xu, H. Zhang, R. Li, H. Shao, W. Lei, Y. Cui, *Chem. Mater.* 2010, **22**, 5838.
26 T. Mahalingam, V. S. John, S. Rajendran, P. J. Sebastian, *Semicond. Sci. Technol.* 2002, **17**, 465.
27 S. K. Choi, U. Kang, S. Lee, D. J. Ham, S. M. Ji, H. Park, *Adv. Energy Mater.* 2014, **4**, 1301614.
28 J. Chen, K. Li, Y. Luo, X. Guo, D. Li, M. Deng, S. Huang, Q. Meng, *Carbon* 2009, **47,** 2704.
29 L. Han, N. Koide, Y. Chiba, A. Islam, R. Komiya, N. Fuke, A. Fukui, R. Yamanaka, *Appl. Phys. Lett.* 2005, **86**, 213501.
30 M. Hu, J. Chen, Z. –Y. Li, L. Au, G. V. Hartland, X. Li, M. Marquez , Y. Xia, *Chem. Soc. Rev.* 2006, **35**, 1084.
31 J. Turkevich, G. Garton, P. C. Stevenson, *J. Colloid Interface Sci.* 1954, **9**, 26.
32 R. H. Doremus, *J. Chem. Phys.* 1964, **40**, 2389.
33 K. L. Shuford, M. A. Ratner, G. C. Schatz, *J. Chem. Phys.* 2005, **123**, 114713-1.
34 J.L. Freeouf, J. M. Woodall, *Appl. Phys. Lett.* 1981, **39**, 727.
35 N. T. Khoa, S. W. Kim, D. –H. Yoo, E. J. Kim, S. H. Hahn, *Appl. Catal. A.* 2014,**469,** 159.
36 Y. Zhang, O. Pluchery, L. Caillard, A. –F. Lamic-Jumblot, S. Casale, Y. J. Chabal. M. Salmeron, *Nano Lett.* 2015, **15**, 51.
37 S. Jeetendra1, H. Nagabhushana, K. Mrudula, C. S. Naveen, P. Raghul, H. M. Mahesh, *Int. J. Electrochem. Sci*. 2014**, 9**, 2944.
38 L. Zhang, D. Zhu, G. M. Nathanson, R. J. Hamers, *Angew. Chem. Int. Ed.* 2014, **53,** 9746.
39 K. Sun, K .Madsen, P. Andersen, W. Bao, Z. Sun, D. Wang, *Nanotechnology*, 2012, **23**, 194013
40 A. Kargar, K. Sun, Y. Jing, C. Choi, H. Jeong, Y. Zhou, K. Madson, P. Naughton, S. Jin, G.Y. Jung, D.Wang, *Nano Lett*. 2013, **13**, 3017

Journal Name ARTICLE

Table of Contents

Selective CO production by Au coupled ZnTe/ZnO in photoelectrochemical CO_2 reduction system

*Y. J. Jang, J.-W. Jang, J. Lee, J.H.Kim,H. Kumagai, J. Lee, T. Minegishi, J. Kubota, K. Domen, J.S. Lee**

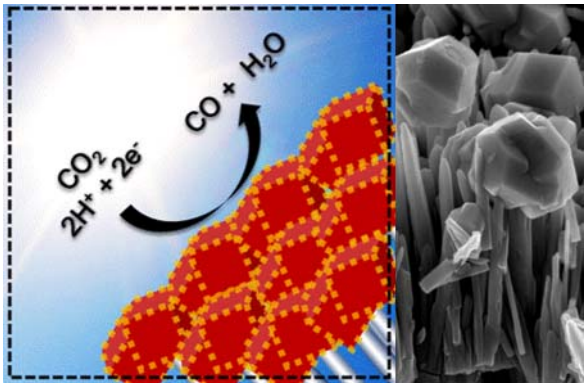

Gold-coupled ZnTe/ZnO-NW array is a new photocathode for selective CO_2 reduction to CO. The remarkable effects of Au co-catalyst are due to formation of a Schottky junction with ZnTe to improve band bending and provide reaction centres of CO_2 reduction suppressing competing water reduction.

Keyword: Zinc Telluride, photocathode, Au nanoparticles, CO_2 reduction, artificial photosynthesis